CHAPTER 3

LAYOUT AND PERFORMANCE

3.1 PERFORMANCE

3.1.1 Performance goals

The Large Hadron Collider (LHC) is a two-ring, superconducting accelerator and collider to be installed in the 27 km long LEP [1] tunnel aiming at the discovery of the Higgs particle and the study of rare events with centre of mass collision energies of up to 14 TeV. The number of events per second generated in the LHC collisions is given by:

$$N_{\mathrm{event}} = L\sigma_{\mathrm{event}} \tag{3.1}$$

where σ_{event} is the cross section for the event under study and L the machine luminosity. The machine luminosity depends only on the beam parameters and can be written for a Gaussian beam distribution as:

$$L = \frac{N_{\mathrm{b}}^2 n_{\mathrm{b}} f_{\mathrm{rev}} \gamma_r}{4\pi\epsilon_n \beta^*} F, \tag{3.2}$$

where N_{b} is the number of particles per bunch, n_{b} the number of bunches per beam, f_{rev} the revolution frequency, γ_{r} the relativistic gamma factor, ϵ_n the normalized transverse beam emittance, β^* the beta function at the collision point and F the geometric luminosity reduction factor due to the crossing angle at the IP:

$$F = 1/\sqrt{1 + \left(\frac{\theta_c \sigma_z}{2\sigma^*}\right)^2}, \tag{3.3}$$

where θ_c is the full crossing angle at the IP, σ_z the RMS bunch length and σ^* the transverse RMS beam size at the IP. (The above expression assumes equal beam parameters for both circulating beams). The exploration of rare events in the LHC collisions therefore requires both high beam energies and high beam intensities.

The LHC has two high luminosity experiments, ATLAS [2] and CMS [3], aiming at a peak luminosity of $L(\mathrm{ATLAS\&CMS}) = 10^{34}$ cm^{-2}s^{-1}. Tabs. 2.1 and 2.2 show the main parameters required to reach a peak luminosity of $L = 10^{34}$ cm^{-2}s^{-1} in the LHC in proton operation. In addition to these high luminosity experiments the LHC has two low luminosity experiments: LHCB [4] for B-physics aiming at a peak luminosity of $L(\mathrm{LHCB}) = 10^{32}$ cm^{-2}s^{-1} and TOTEM [5] for the detection of protons from elastic scattering at small angles aiming at a peak luminosity of $L = 2\times10^{29}$ cm^{-2}s^{-1} with 156 bunches. In addition to the proton beams the LHC will also be operated with ion beams. The LHC has one dedicated ion experiment ALICE [6] aiming at a peak luminosity of $L(\mathrm{ALICE}) = 10^{27}$ cm^{-2}s^{-1} for nominal Pb-Pb ion operation [6]. The parameters required for Pb ion operation are summarized in Chap. 21.

The high beam intensities implied by a luminosity of $L = 10^{34}$ cm^{-2}s^{-1} exclude the use of anti-proton beams and one common vacuum and magnet system for both circulating beams (as it is done in the TEVATRON) and implies the use of two proton beams. To collide two beams of equally charged particles requires opposite magnet dipole fields in both beams. The LHC is therefore designed as a proton-proton collider with separate magnet fields and vacuum chambers in the main arcs and with common sections only at the insertion regions where the experimental detectors are located. The two beams share an approximately 130 m long common beam pipe along the interaction regions (IR). The exact length is 126 m in IR2 and IR8 which feature superconducting separation dipole magnets next to the triplet assemblies and 140 m in IR1 and IR5 which feature normal conducting and therefore longer separation dipole magnets next to the triplet assemblies. Together with the large number of bunches (2808 for each proton beam), and a nominal bunch spacing of 25 ns, the long common beam pipe implies 34 parasitic collision points for each experimental insertion region (for four experimental IR's this implies a total of 136 unwanted collision points). Dedicated crossing angle orbit bumps separate the two LHC beams left and right from the central interaction point (IP) in order to avoid collisions at these parasitic collision points.

There is not enough room for two separate rings of magnets in the LEP tunnel. Therefore the LHC uses twin bore magnets which consist of two sets of coils and beam channels within the same mechanical structure and cryostat.

The peak beam energy in a storage ring depends on the integrated dipole field along the storage ring circumference. Aiming at peak beam energies of up to 7 TeV inside the existing LEP tunnel implies a peak dipole field of 8.33 T and the use of superconducting magnet technology.

3.1.2 Performance limitations for the LHC

The LHC machine performance is limited by seven main effects.

Beam-Beam limit

The maximum particles density per bunch is limited by the nonlinear beam-beam interaction that each particle experiences when the bunches of both beams collide with each other in the IR's. The beam-beam interaction is measured by the linear tune shift given by:

$$\xi = \frac{N_{\mathrm{bunch}} r_p}{4\pi\epsilon_n}, \tag{3.4}$$

where r_p is the classical proton radius $r_p = e^2/(4\pi\epsilon_0 m_p c^2)$. Experience with existing hadron collider machines indicates that the total linear tune shift (sum of all IP's) should not exceed 0.015. With three proton experiments requiring head-on collisions this implies that the linear beam-beam tune shift for each IP should satisfy $\xi \leq 0.005$. A detailed discussion of the limitations due to the beam-beam interaction can be found in Section 5.08.

Mechanical aperture

The geometrical aperture of the LHC arcs is given by the beam screen dimensions. The beam screen has a height of approximately 2×17.3 mm and a total width of 2×22 mm (a detailed description of the LHC beam screen is given in Chap. 12). Requiring a minimum aperture of $10\ \sigma$ in terms of the RMS beam sizes and assuming tolerances for the linear machine imperfections and the magnet alignment and geometry implies a peak nominal beam size of 1.2 mm (a minimum mechanical aperture of $10\ \sigma$ is prescribed by the LHC beam cleaning system which is described in more detail in Chap. 18). A detailed list of the assumed optics and mechanical imperfections is given in Sec. 4.03. Combined with a peak β-function of 180 m in the LHC arcs this implies a maximum acceptable transverse beam emittance of $\epsilon_n = 3.75\ \mu$m. Combined with the limit on the linear beam-beam tune shift the mechanical aperture of the LHC therefore limits the maximum bunch intensity to $N_{\mathrm{bunch}}(\mathrm{nominal}) = 1.15 \times 10^{11}$.

Furthermore, the mechanical aperture of the triplet magnets limits the minimum attainable β^* value at the IP's and the maximum attainable crossing angle orbit bump in the experimental IR's. Both parameters can limit the peak luminosity in the LHC machine. A detailed description of the IR magnet parameters can be found in Chap. 8 and a description of the luminosity limitations due to the mechanical aperture in the IR's in Chap. 5.

Maximum dipole field and Magnet quench limits

The maximum γ_{r} that can be reached in the LHC is limited by the peak dipole field in the storage ring. The nominal field is 8.33 T corresponding to a beam energy of 7 TeV. However, the actual field attainable in the storage ring depends on the heat load and temperature margins inside the cryo-magnets and therefore on the beam losses in the machine during operation. A high dipole field therefore implies efficient operation with minimum beam losses. A detailed description of the limitations for the peak dipole field and the beam losses can be found in Chaps. 7 and 18.

Energy stored in the circulating beams and in the magnetic fields

A total beam current of 0.584 A corresponds to a stored energy of approximately 362 MJ. In addition to the energy stored in the circulating beams the LHC magnet system has a stored electromagnetic energy of

approximately 600 MJ yielding a total stored energy of more than 1 GJ. This stored energy must be absorbed safely at the end of each run or in the case of a malfunction or an emergency. The beam dumping system and the magnet system therefore provide additional limits for the maximum attainable beam energies and intensities (see Chaps. 7 and 17 for details on the above limits).

Heat load

Although the synchrotron radiation in hadron storage rings is small compared to that generated in electron rings it can still impose practical limits to the maximum attainable beam intensities if the radiation must be absorbed in a cryogenic system. In addition to the heat load due to synchrotron radiation, the LHC cryogenics system must absorb the heat deposition from luminosity induced losses in the IR and the impedance issues (resistive wall effect) and electron cloud bombardment. The latter two effects are described in detail in Chap. 5.

Field quality and dynamic aperture

Field quality errors spoil the particle stability in the storage ring and loss-free operation of the machine therefore requires a high field quality. A characterizing feature of superconducting magnets is the decay of persistent currents and their 'snap back' at the beginning of the ramp. Small beam losses therefore require a tight control of the magnet field errors during magnet production and during machine operation. Assuming fixed limits for the beam losses due to the quench levels of the superconducting magnets, the accuracy of the field quality correction during operation limits the maximum attainable machine performance. A detailed description of the required magnet field quality can be found in Chap. 4. A description of the time dependent effects in superconducting magnets and the reference system for their correction during operation is given in Chaps. 7 and 20 while a discussion of the beam instrumentation available for beam based corrections of the field errors in Chap. 13.

Collective beam instabilities

The interaction of the charged particles in each beam with each other via electromagnetic fields and the conducting boundaries of the vacuum system can result in collective beam instabilities. Generally speaking the collective effects are a function of the vacuum system geometry and its surface properties. They are usually proportional to the beam currents and can therefore limit the maximum attainable beam intensities in the LHC beams. A detailed discussion of the collective effects in the LHC can be found in Chap. 5. High beam and bunch intensities, as implied by the nominal design luminosity for the LHC, therefore imply tight control of the vacuum system cross sections and surface properties. Both aspects are discussed in Chap. 12.

3.1.3 Luminosity lifetime

The luminosity in the LHC is not constant over a physics run but decays due to the degradation of intensities and emittances of the circulating beams.

The main cause for the luminosity decay for nominal LHC performance are the collisions themselves. The initial decay time of the bunch intensity, due to this effect, is:

$$\tau_{\mathrm{nuclear}} = \frac{N_{\mathrm{tot},0}}{L\sigma_{\mathrm{tot}}k}, \tag{3.5}$$

where $N_{\mathrm{tot},0}$ is the initial beam intensity, L the initial luminosity, σ_{tot} the total cross section ($\sigma_{\mathrm{tot}} = 10^{-25}$ cm^2 at 7 TeV) and k the number of interaction points. Assuming an initial peak luminosity of $L = 10^{34}$ cm^{-2}s^{-1} and two high luminosity experiments the above expression yields an initial decay time of $\tau = 44.85$ h.

Eq. (3.5) results in the following decay of the beam intensity and luminosity as functions of time [7]:

$$N_{\mathrm{tot}}(t) = \frac{N_{\mathrm{tot},0}}{1 + t/\tau_{\mathrm{nuclear}}} \tag{3.6}$$

$$L(t) = \frac{L_0}{(1 + t/\tau_{\mathrm{nuclear}})^2}. \tag{3.7}$$

The time required to reach 1/e of the initial luminosity is given by [7]:

$$t_{1/e} = (\sqrt{e} - 1)\tau. \tag{3.8}$$

yielding a luminosity decay time of $\tau_{\mathrm{nuclear},1/e} = 29$ h.

Other contributions to beam losses come from Toucheck scattering and from particle losses due to a slow emittance blow-up. An emittance blow-up can be caused by the scattering of particles on the residual gas, the nonlinear force of the beam-beam interaction, RF noise and IBS scattering effects.

The synchrotron radiation damping in the LHC decreases the bunch dimensions at top energy and can partially compensate the beam size blow-up due to the above effects. Following the arguments set out in the Pink Book (the 1991 Design Study) [8] we assume here that the radiation damping process just cancels the beam blow up due to the beam-beam interactions and RF noise. Approximating further the decay due to the beam-beam interaction by an exponential decay process [9] one can estimate the net luminosity lifetime by:

$$\frac{1}{\tau_L} = \frac{1}{\tau_{\mathrm{IBS}}} + \frac{2}{\tau_{\mathrm{rest-gas}}} + \frac{1}{\tau_{\mathrm{nuclear},1/e}}. \tag{3.9}$$

Inserting the exponential nuclear decay time, a transverse IBS growth time of $\tau_{\mathrm{IBS}} = 80$ h (see Chap. 5 for more details on the IBS growth time estimates) and a vacuum beam lifetime of $\tau_{\mathrm{rest-gas}} = 100$ h [10] (see Chap. 12 for more details on the vacuum beam lifetime estimates) on obtains a net luminosity lifetime of:

$$\tau_L = 14.9 \text{ h}. \tag{3.10}$$

3.1.4 Integrated luminosity

Estimating the integrated luminosity of a storage ring requires assumptions on the average turnaround time of the storage ring and the average number of luminosity fills per year. Having no operational data available for LHC, data from the HERA proton ring operation will be used as a reference [11].

3.1.5 Average Turnaround Time

Filling the LHC requires 12 cycles of the SPS synchrotron and each SPS fill requires 3 to 4 cycles of the PS synchrotron. The SPS and PS cycling time are 21.6 and 3.6 s respectively, yielding a total LHC filling time of approximately 4 mins per beam. Assuming that each LHC aperture requires additional 4 SPS cycles for the injection set up (3 pilot bunches and one nominal intensity) and that the LHC operators require at least 2 mins to evaluate the measurements of each pilot bunch shots and to readjust the machine settings, the total (minimum) LHC injection time becomes:

$$T_{\mathrm{inj}}(LHC) \approx 16 \text{ min}. \tag{3.11}$$

The minimum time required for ramping the beam energy in the LHC from 450 GeV to 7 TeV is approximately 20 minutes [12]. After a beam abort at top energy it takes also approximately 20 mins to ramp the magnets down to 450 GeV. Assuming a programmed check of all main systems of 10 mins [8] one obtains a total turnaround time for the LHC of [1]:

$$T_{\mathrm{turnaround,min}}(LHC) \approx 70\text{min}. \tag{3.12}$$

After 10 years of machine operation, on average, only every third proton injection in HERA leads to a successful proton fill at top energy [13]. The average time between the end of a luminosity run and a new beam at top energy in HERA is approximately 6 h compared to a theoretical minimum turnaround time of approximately 1 h. In the following analysis we consider therefore two cases for evaluating the integrated machine luminosity: i) the minimum theoretical turnaround time of the LHC, i.e. $T_{\mathrm{turnaround}}(\mathrm{case1}) = 1.2$ h and ii) a turnaround time which is 6 times larger than the minimum theoretical turnaround time, i.e. $T_{\mathrm{turnaround}}(\mathrm{case2}) = 7$ h.

[1] The pink book quotes a minimum turnaround time of 2 hours [8].

3.1.6 Integrated Luminosity

Integrating the luminosity over one luminosity run yields:

$$L_{\rm int} = L_0 \tau_L [1 - e^{-T_{run}/\tau_L}] \tag{3.13}$$

where $T_{\rm run}$ is the total length of the luminosity run.

The overall collider efficiency depends on the ratio of the run length and the average turnaround time. Assuming that the machine can be operated during 200 days per year the total luminosity per year is given by:

$$L_{\rm tot} = \frac{200 \times 24}{T_{\rm run}[h] + T_{\rm turnaround}[\rm h]} L_{\rm int}. \tag{3.14}$$

The total luminosity per year attains a maximum if the run time satisfies the following equation

$$ln(\frac{T_{\rm turnaround} + T_{\rm run}}{\tau_L} + 1) = \frac{T_{\rm run}}{\tau_L}. \tag{3.15}$$

Assuming a luminosity lifetime of 15 h one obtains optimum run times of 12 h and 5.5 h for an average turnaround time of 7 h and 1.2 h, respectively. Inserting the nominal peak LHC luminosity and the optimum run times into Eqs. (3.13) and (3.14) one obtains for the maximum total luminosity per year between 80 fb^{-1} and 120 fb^{-1} depending on the average turn around time of the machine.

3.2 LATTICE LAYOUT

All lattice descriptions in this Chapter refer to the LHC Version 6.4 including the repositioning [1] of the Q3 triplet magnets which is part of Version 6.5. [2]

3.2.1 The LHC in the LEP tunnel

The basic layout of the LHC follows the LEP tunnel geometry and is depicted in Fig.3.2. The LHC has eight arcs and straight sections. Each straight section is approximately 528 m long and can serve as an experimental or utility insertion. The two high luminosity experimental insertions are located at diametrically opposite straight sections: the ATLAS experiment is located at point 1 and the CMS experiment at point 5. Two more experimental insertions are located at point 2 and point 8 which also contain the injection systems for Beam 1 and Beam 2, respectively. The injection kick occurs in the vertical plane with the two beams arriving at the LHC from below the LHC reference plane. The beams only cross from one magnet bore to the other at these four locations. The remaining four straight sections do not have beam crossings. Insertion 3 and 7 each contain two collimation systems. Insertion 4 contains two RF systems: one independent system for each LHC beam. The straight section at point 6 contains the beam dump insertion where the two beams are vertically extracted from the machine using a combination of horizontally deflecting fast-pulsed ('kicker') magnets and vertically-deflecting double steel septum magnets. Each beam features an independent abort system.

The LHC lattice has evolved over several versions. The Conceptual Design Report [14] was based on lattice version 4 which did not provide the required flexibility for the optics design. Significant improvements were introduced in version 5 and 6 of the LHC lattice [15] and [16] summarizes their main benefits. A summary of the different LHC lattice versions is given in [17].

The arcs of LHC lattice version 6.4 are made of 23 regular arc cells. The arc cells are 106.9 m long and are made out of two 53.45 m long half cells each of which contains one 5.355 m long cold mass (6.63 m long cryostat) short straight section (SSS) assembly and three 14.3 m long dipole magnets. The LHC arc cell has been optimized for a maximum integrated dipole field along the arc with a minimum number of magnet interconnections and with the smallest possible beam envelopes [18]. Fig. 3.1 shows a schematic picture of one LHC half-cell and Sec. 3.2.3 explains the functionality of the SSS in detail. The two apertures for Ring

[2] A summary of the differences between different LHC lattice versions can be found on the WWW under: http://slap.web.cern.ch/slap/MAC.pdf

1 and Ring 2 are separated by 194 mm. The two coils in the dipole magnets are powered in series and all dipole magnets of one arc form one electrical circuit. The quadrupoles of each arc form two electrical circuits: all focusing quadrupole magnets in Ring 1 and Ring 2 are powered in series and all defocusing quadrupole magnets of Beam 1 and Beam 2 are powered in series. The optics of Beam 1 and Beam 2 in the arc cells is therefore strictly coupled via the powering of the main magnetic elements.

A dispersion suppressor is located at the transition between an LHC arc and a straight section yielding a total of 16 dispersion suppressor sections. The aim of the dispersion suppressors is threefold [16]:

- adapt the LHC reference orbit to the geometry of the LEP tunnel;
- cancel the horizontal dispersion arising in the arc and generated by the separation / recombination dipole magnets and the crossing angle bumps;
- help in matching the insertion optics to the periodic solution of the arc.

A generic design of a dispersion suppressor uses standard arc cells with missing dipole magnets [19]. The LEP dispersion suppressor, which defines the geometry of the tunnel, was made of 3.5 cells with a 90° phase advance, optimized to suppress the dispersion. With the 2.5 times longer LHC dipole and quadrupole magnets, only two LHC cells can be fitted in the dispersion suppressor tunnel.

This layout can still accurately follow the LEP tunnel (see Sec 3.2.2). However, the shortened dispersion suppressor cannot fully cancel the horizontal dispersion if the dispersion suppressor cells are powered in series with the arc cells. Relying only on the missing dipole concept for the dispersion suppression the horizontal arc dispersion can only be reduced by a factor of 2.5 [20]. Full cancellation of the horizontal dispersion requires individual powering of the dispersion suppressor quadrupole magnets. To this end the dispersion suppressor cells are equipped with special, medium current, quadrupole magnets. A detailed description of the special insertion quadrupole magnets can be found in Chaps. 8 and 10. Fig. 3.3 shows the schematic layout of the LHC dispersion suppressors. The only exceptions to the above layout are IR3 and IR7 which do not have enough space to house the large 6000 A power supplies required for individual powering of the dispersion suppressor quadrupole magnets. Instead, the dispersion suppressor quadrupole magnets in IR3 and IR7 are powered in series with the arc quadrupole magnets and each dispersion suppressor quadrupole is equipped with a trim quadrupole magnet that requires only a small 500 A power supply. This solution solves the problem of limited space in the underground alcoves but limits the flexibility for the IR3 and IR7 dispersion suppressor insertions. Sec 3.2.6 describes in detail the consequences of the insertion quadrupole powering in IR3 and IR7.

The long straight sections in the LEP tunnel are approximately 528 m long. Assuming a quadrupole magnet spacing equivalent to the magnet separation in the LHC arc cells, provides sufficient space for approximately 10 insertion region quadrupole magnets. The exact number and arrangement of these quadrupole magnets in the insertion region might be further restricted by the special requirements in each insertion. Sec 3.2.4 to 3.2.9 describe the detailed insertion layout for each insertion type. Assuming a midpoint symmetry for the insertion optics this provides 5 independent parameters for matching 6 optics constraints (β_x, β_y, α_x, α_y, μ_x, and μ_y) at the transition points to the dispersion suppressors (assuming that the dispersion functions can be matched via the dispersion suppressor parameters). Even without additional optics constraints from the insertion region this minimum number of constraints exceeds the number of free parameters (Secs. 3.2.4 to 3.2.9 describe in detail the special requirements for each LHC insertion). [3] The dispersion suppressor therefore has to act as an optical buffer between the arc and the insertion optics which provides additional parameters for matching the insertion optics. In order to cope with this additional functionality the dispersion suppressors are extended into the neighboring arcs using the arc trim quadrupole magnets of the first arc cell next to each dispersion suppressor. This procedure adds four more parameters for matching the insertion optics to the arc (two parameters for each dispersion suppressor). The drawback of the above implementation is that it does not provide strictly separated functionality of the dispersion suppressor and the insertion regions.

[3] Up to Version 4 of the LHC lattice the experimental insertion featured only 4 functional quadrupole units on each side of the IP: an inner triplet powered in series as one unit left and right from the IP and an 'outer triplet' of three individually powered insertion quadrupole magnets on each side of the IP.

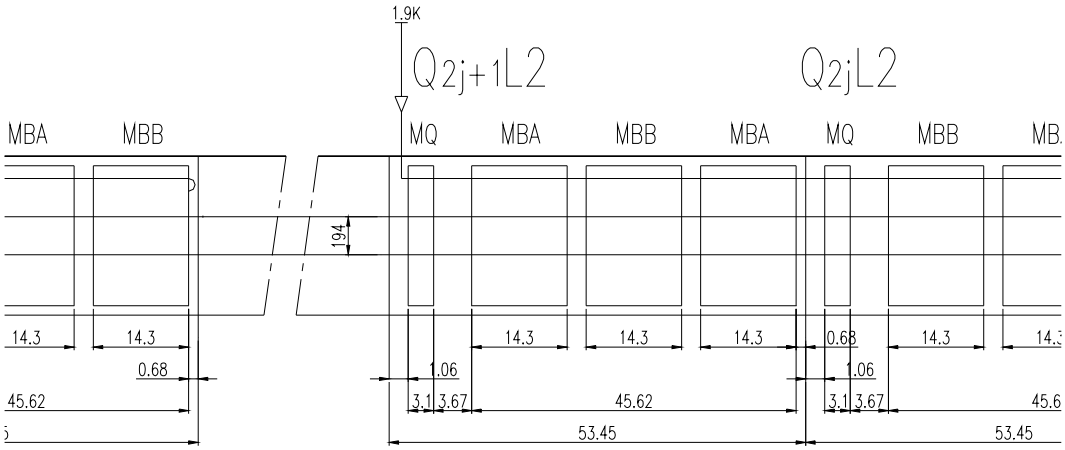

Figure 3.1: Schematic layout of an LHC half-cell

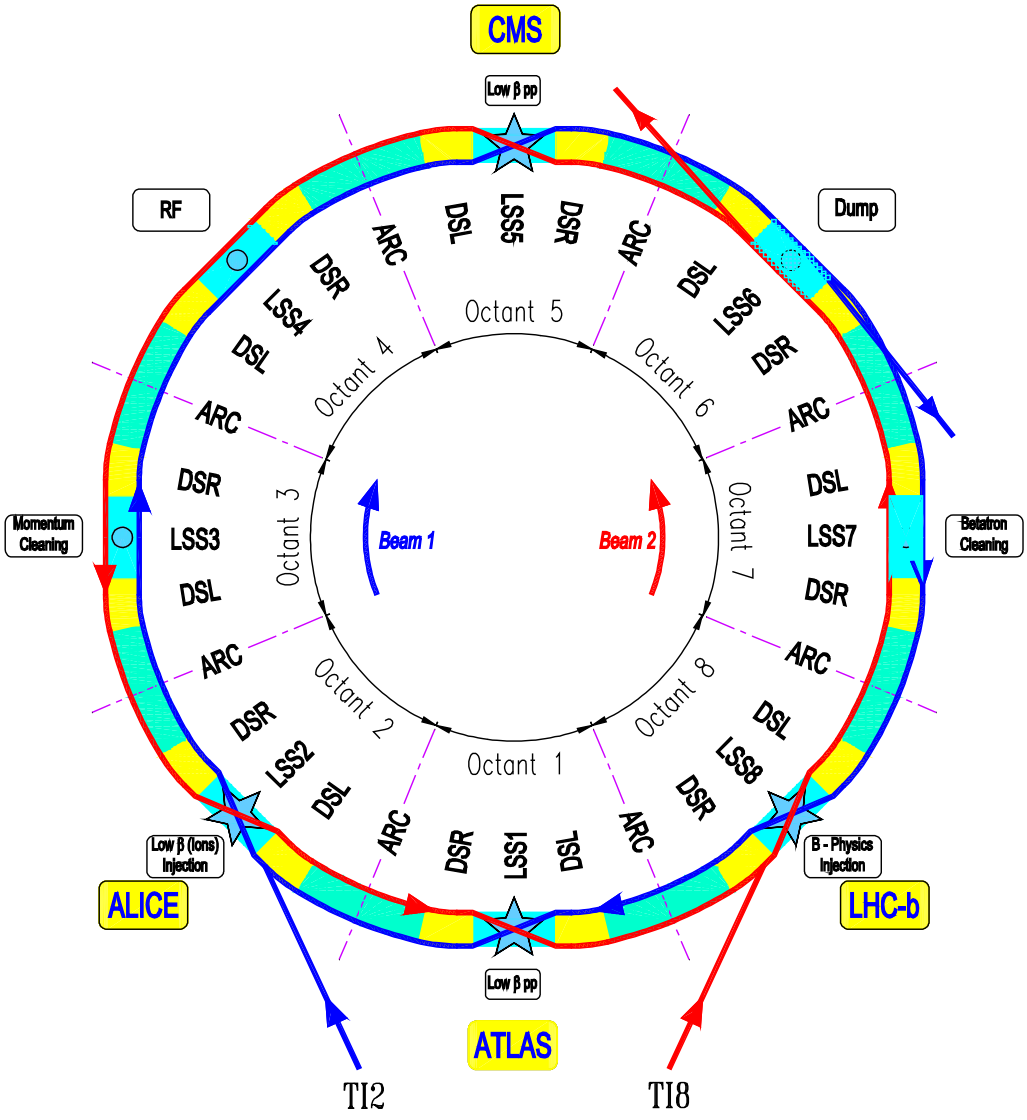

Figure 3.2: Schematic layout of the LHC. Beam 1 circulates clockwise and Beam 2 counter-clockwise.

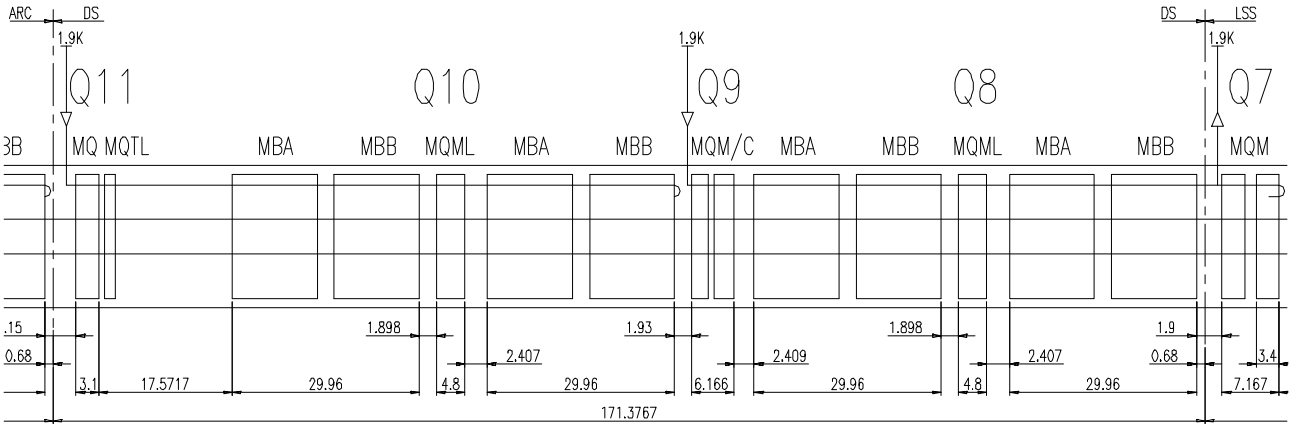

Figure 3.3: Schematic layout of LHC dispersion suppressor next to IR2

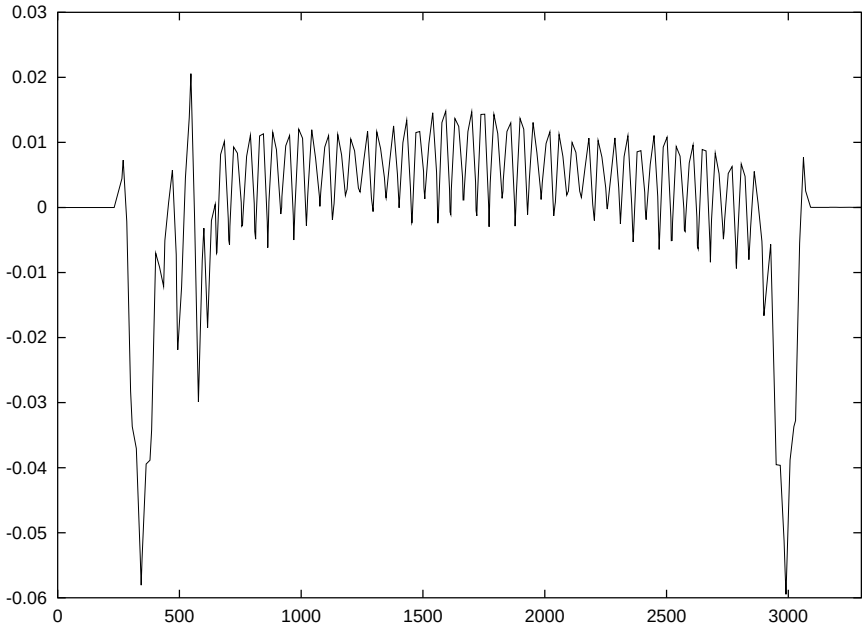

Figure 3.4: The horizontal position of the LHC compared to the LEP in one sector of the machine in metres.

3.2.2 Geometry

The LHC arcs tend to be radially exterior to the theoretical position of the LEP machine by up to 4 cm with the maximum excursions occurring near the arc transition to the dispersion suppressor. The total LHC circumference is kept equal to the LEP circumference and the positive offset of the LHC machine in the arcs is compensated by a larger excursion in the opposite direction inside the dispersion suppressor. The offset in the dispersion suppressor region reaches up to -0.1 m and is caused by the mismatch of the long LHC cells and the relatively short LEP dispersion suppressor section. Fig. 3.4 shows the horizontal position of the LHC compared to the LEP in one sector of the machine in metres.

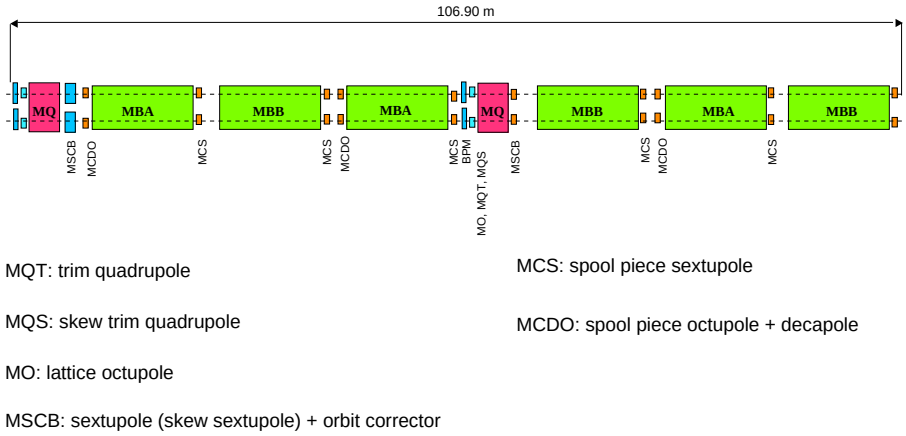

Figure 3.5: Schematic layout of the LHC arc corrector magnets

3.2.3 Functional description of the arc corrector circuits

The LHC correction circuits have evolved over the different LHC lattice versions [21][16]. The circuit description given in this Section is based on the LHC lattice version 6.4.

The corrector magnets located in the arcs of the LHC can be split into two distinct categories (see Fig. 3.5):

- The lattice corrector magnets attached on both sides of the main quadrupole magnets are installed in the Short Straight Section (SSS) cryostats.
- The spool-piece corrector magnets which are thin non-linear windings attached directly on the extremities of the main dipoles.

Contrary to the main dipole circuits and the two families (QF and QD) of lattice quadrupoles for which, in each sector, Ring 1 and Ring 2 are powered in series, the arc corrector magnets can be adjusted independently for the two beams.
The different types and main functionalities of the lattice corrector magnets are summarized below.

Arc orbit corrector magnets MCB

Horizontal and vertical orbit corrector magnets, MCBH and MCBV, are installed at each focusing (QF) and defocusing (QD) quadrupole, respectively, that is a total of 23 or 24 orbit correctors per ring, per arc and per transverse plane, depending on the polarity of the quadrupole at mid-arc. They are designed to achieve a maximum kick of $80.8\,\mu$rad at 7 TeV for a nominal current of 55 A (see for example, [22]).

Chromaticity or lattice sextupoles, MS

Chromaticity sextupoles, MS, will be installed at each focusing and defocusing quadrupole of the lattice. In a previous design these magnets were combined with the orbit corrector magnets MCB. The two windings are now well separated in the so-called MSCB assembly. The chromaticity sextupoles are split into four families in

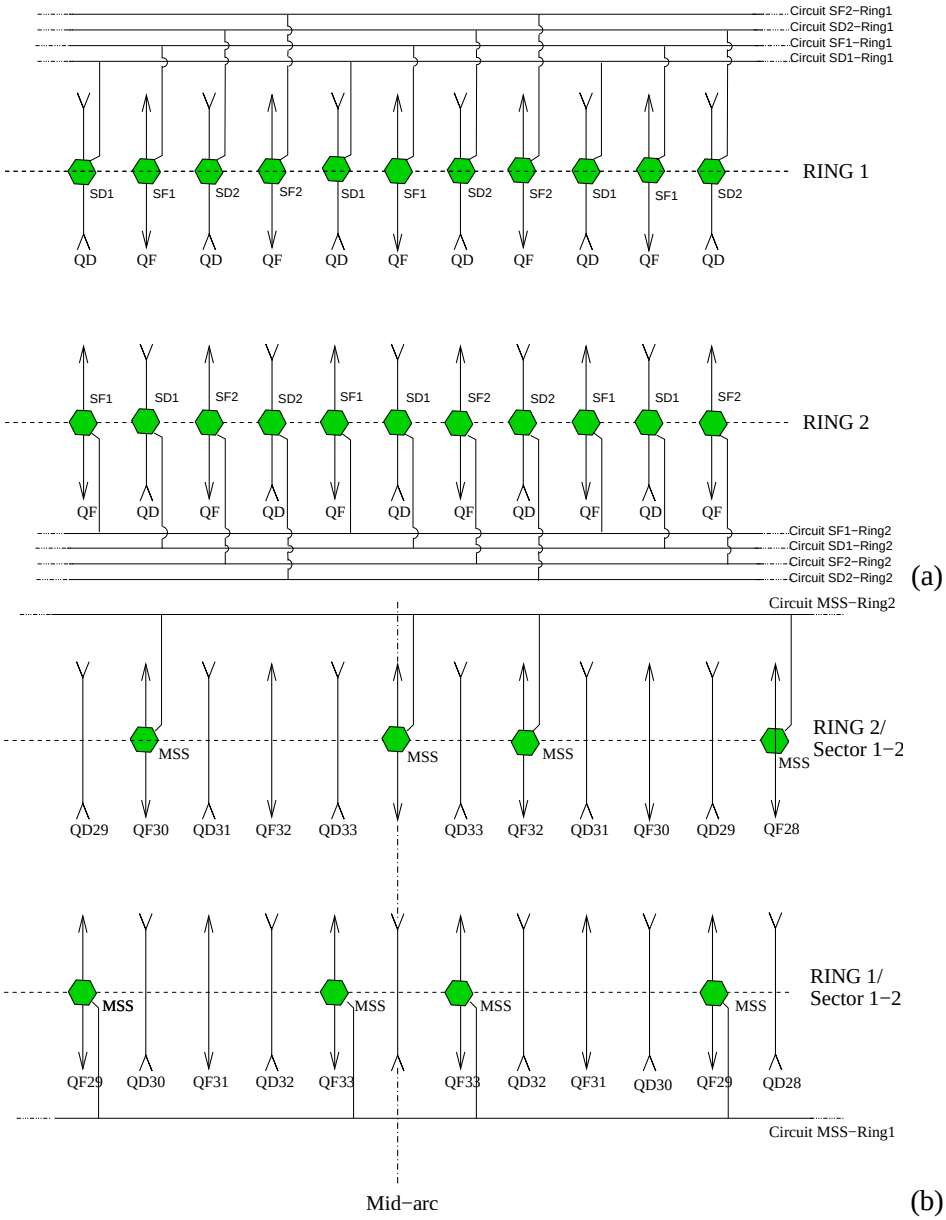

Figure 3.6: Arrangement in four families per ring and per sector for the chromaticity sextupoles MS in the LHC arcs (top) and dedicated location for the skew sextupole corrector MSS around the mid-arc in the case of Sector 1-2 (bottom).

each sector of each ring: that is two families, SF and SD installed at QF and QD, respectively. These are further divided into two interleaved sub-families '1' and '2' (see Fig. 3.6(a)). Only two SF and SD families are needed to correct the natural chromaticity of each ring. This includes the contributions from the arc ($Q'_{\mathrm{nat.}} \sim -80$) and/or the contribution from the low-β insertions in collision ($Q'_{\mathrm{nat.}} \sim -30$ for one experimental insertion squeezed to $\beta^* = 0.55$ m). Thanks to the phase advance close to 90° in the LHC arc cell, the present scheme has been designed to correct also the second order chromaticity $Q''_{x,y}$ and to minimize the off-momentum β-beating induced by the triplet magnets in collision (see [23] and [24] for more detail).
Note that the SF's and SD's are made of the same corrector magnets. Therefore, the integrated strength of the SD's sets the ultimate performance of the system as the dispersion function is smaller by a factor 2 compared to its value at the SF's.

Lattice skew sextupoles, MSS

In each ring and each sector of the machine, four focusing sextupoles (more precisely 2 SF1's and 2 SF2's) are tilted by 90° and are powered in series to generate a skew sextupole field for a compensation of the chromatic coupling induced by the a_3 component of the main dipoles. The MSS magnets are installed at Q29-Q33-Q33-Q29 in the sectors 1-2, 3-4, 5-6, 7-8 of Ring 1 (where the mid-arc quadrupole Q34 is defocusing for Beam 1) and in the sectors 2-3, 4-5, 6-7, 8-1 of Ring 2 (where Q34 is defocusing for Beam 2). For all other sectors they are installed at Q30-Q34-Q32-Q28 (see Fig. 3.6(b)). Such a scheme guarantees an extremely good compensation of the second order chromaticity induced by chromatic coupling with a minimum impact on the third order skew resonances and on the off-momentum β-beating (see [25] for more detail). Finally, as for the SF correction circuits, the efficiency of the MSS magnets is also doubled in terms of required strength since they are systematically installed close to a focusing quadrupole QF.

Tune-shift or tuning quadrupoles, MQT

Two families of 8 tuning quadrupoles per ring and per sector, QTF and QTD, equip the short-straight sections from Q14 to Q21 (left and right). Since the main quadrupole circuits are powered in series in Ring 1 and Ring 2, the phase advance per arc cell cannot be changed independently for the two rings. Therefore, independent tune adjustments for both beams can only be done by re-tuning the phase advances of the LHC insertions (essentially IR4, see Sec. 4.2.5) or by using the MQT corrector magnets. In principle, the latter are strong enough to achieve tune shifts of slightly more than one unit at 7 TeV. However, due to the large β-beating and dispersion mismatch induced they will be limited to much smaller tune shifts in nominal operation, of the order to $\Delta Q \sim \pm 0.1$ (see [26] for more detail).

Arc skew quadrupole corrector magnets, MQS

In both of the rings, each sector of the machine is equipped with 2 pairs of skew quadrupole magnets MQS at Q23 and Q27 (left and right) which are just MQT type magnets tilted by 45°. The two pairs are either powered in series, in sectors 1-2, 3-4, 5-6, 7-8 for Ring 1 and in sectors 2-3, 4-5, 6-7, 8-1 for Ring 2, or split into two independent families in the other sectors. This layout allows compensation of the coupling coefficient due to the systematic a_2 errors of the main dipoles for each sector but implies that only four corrector circuits are available for correction of the random coupling errors. Furthermore, the betatron phase advances between the MQS's of a same family ensures that the coupling compensation can be made without generating too large a vertical dispersion and with a minimum excitation of the sum coupling resonance, in order to minimize the β-beating possibly induced by the correction (see [27]).

Landau damping or lattice octupoles, MO

Each short straight section not equipped with MQT or MQS type magnets contains a lattice octupole MO, making a total of 168 MO type magnets per ring. These magnets will be powered in four families per sector, subdividing them into focusing and defocusing magnets, OF and OD, for Ring 1 and Ring 2. Assumed to have zero field at injection, the latter will Landau damp the coherent oscillations caused by collective effects [28].

Spool-piece corrector magnets

In addition to the lattice corrector magnets, each bore of the main dipoles will carry a small sextupole corrector magnet (MCS) at one end (Type B magnet) and every other dipole will be equipped with an octupole-decapole spool-piece (MCDO) at the opposite end (Type A magnet). The MCS magnets will be connected in series to form two families per sector, one for each ring. The same will apply for the octupole and decapole corrector magnets.
The MCS spool-pieces are designed to compensate the b_3 field integral of the main dipoles in each sector of the machine in order to correct its impact on the linear chromaticity up to the top energy. On the other hand the

Table 3.1: Arc corrector families and strength budget for the LHC Version 6.

Type	Name	Mag. length [m]	Nominal current [A]	Nominal field [T] at $R_r = 17$ mm	Family name	Number of families per ring	Number of magnets per ring	Max. integrated strength per ring at 450 GeV / 7 TeV
Lattice corrector magnets								
b_1 a_1	MCB	0.650	55	2.900	RCBH RCBV	188 188	188 188	376 / 24.17 units
b_2	MQT	0.320	550	2.040 (120 T/m)	RQTF RQTD	8 8	64 64	44.3 / 2.85 units
a_2	MQS	0.320	550	2.040 (120 T/m)	RQS	12	32	22.2 / 1.42 units
b_3	MS	0.369	550	1.280	RSF (SF1 & SF2) RSD (SD1 & SD2)	16 16	156 188	78.2 / 5.03 units 94.3 / 6.06 units
a_3	MSS	0.369	550	1.280	RSS	8	32	16.0 / 1.03 units
b_4	MO	0.320	550	0.290	ROF ROD	8 8	84 84	8.27 / 0.53 units
Spool-piece corrector magnets								
b_3	MCS	0.110	550	0.471	RCS	8	1232	67.7 / 4.35 units
b_4	MCO	0.066	100	0.040	RCO	8	616	1.73 / 0.11 units
b_5	MCD	0.066	550	0.100	RCD	8	616	4.31 / 0.28 units

MCDO spool-piece corrector magnets mainly preserve the dynamic aperture of the LHC at injection.

Corrector strength

The nominal strength of each arc corrector magnet is reported in Tab 3.1. In order to compare with the field imperfections of the main dipoles, the integrated strength per ring of each correction circuit has also been expressed in units of 10^{-4} relative field error in the main dipoles at a reference radius of $R_r = 17$ mm:

$$(BL)_{\mathrm{Ring}}\,(x = 17\,\mathrm{mm}) = 1\,\mathrm{Tm}$$
$$\leftrightarrow$$
$$(BL)_{\mathrm{Ring}} = \frac{1}{2\pi\,B\rho} \times 10^4 = \begin{cases} 1.061 \text{ units at 450 GeV} \\ 0.068 \text{ units at 7 TeV.} \end{cases}$$

With the exception of the multipoles b_3, b_4, b_5 for which the correction strategy consists effectively in a compensation of the field imperfection integrated per arc, the last column of Tab 3.1 is just indicative and generally underestimates the efficiency of the different correction circuits.

3.2.4 IR1 and IR5

General description

IR1 and IR5 house the high luminosity experiments of the LHC and are identical in terms of hardware and optics (except for the crossing-angle scheme: the crossing angle in IR1 is in the vertical plane and in IR5 in the horizontal plane). The small β-function values at the IP are generated with the help of a triplet quadrupole assembly [19]. A detailed description of the matching constraints for IR1 and IR5 can be found in [29]. The free space around the IPs is ± 23 m and the Q1 magnet stands in the tunnel instead of being supported by a cantilever inside the experimental cavern. At the IP, the two rings share the same vacuum chamber, the same low-beta triplet magnets and the D1 separation dipole magnets. The remaining matching section (MS) and the dispersion suppressor (DS) consist of double-bore magnets with separate beam pipes for each ring.

IR layout

Apart from the DS the insertions are comprised of the following sections, given in order from the interaction point:

- A 31 m long superconducting low-β triplet assembly operated at a temperature of 1.9 K and providing a nominal gradient of 205 T/m.
- A pair of separation / recombination dipoles separated by approximately 88 m. The D1 dipole located next to the triplet magnets has a single bore and consists of six 3.4 m long conventional warm magnet modules yielding a nominal field of 1.38 T. The following D2 dipole is a 9.45 m long, double bore, superconducting dipole magnet operating at a cryogenic temperature of 4.5 K with a nominal field of 3.8 T. The bore separation in the D2 magnet is 188 mm and is thus slightly smaller than the arc bore separation.
- Four matching quadrupole magnets. The first quadrupole following the separation dipole magnets, Q4, is a wide-aperture magnet operating at a cryogenic temperature of 4.5 K and yielding a nominal gradient of 160 T/m. The remaining three quadrupole magnets are normal-aperture quadrupole magnets operating at a cryogenic temperature of 1.9 K with a nominal gradient of 200 T/m.

Fig. 3.7 shows the schematic layout of IR1 and Tab 3.2 summarizes its main hardware parameters.

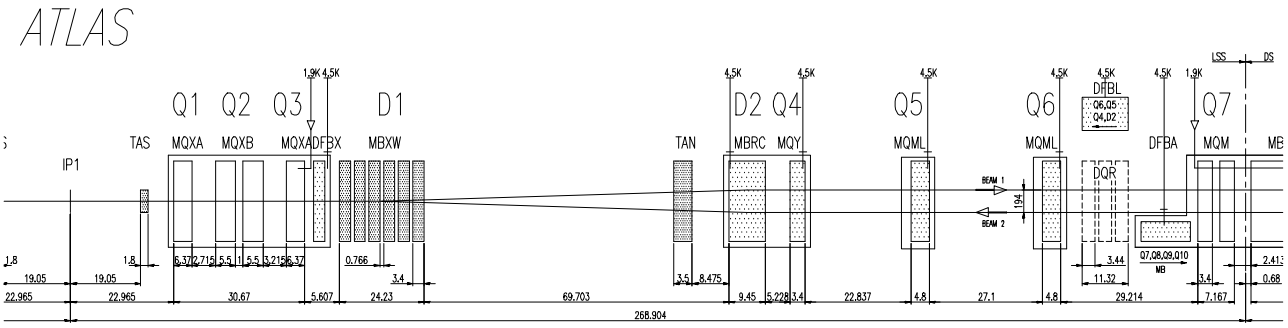

Figure 3.7: Schematic layout of the right side of IR1

Table 3.2: *Magnet parameters in IR1 and IR5.*

	LSS							Optical DS					
	low-β triplet			MS				DS				arc-cell	
Magnet	Q1	Q2	Q3	Q4	Q5	Q6	Q7	Q8	Q9	Q10	QT11	QT12	QT13
#	1	2	1	1	1	1	2	1	2	1	1	1	1
Type: MQ-	XL	X	XL	Y	ML		M	ML	M C	ML	TL	T	
L [m]	6.3	5.5	6.3	3.4	4.8	4.8	3.4	4.8	3.4 2.4	4.8	1.15	0.32	0.32
T [K]	1.9			4.5			1.9	1.9				1.9	
G [T/m]	200/205			160			200	200			110	110	
r [mm]	22.2 v17.3	28.95 24.05		27.2 22.3	20.6 15.75		22.2 17.3	22.2 17.3				22.2 17.3	

The triplet assembly features two different quadrupole designs: the outer two quadrupole magnets are made by KEK and require a peak current of 6450 A to reach the nominal gradient of 205 T/m, whereas the inner quadrupole block consists of two quadrupole magnets made by FNAL and requires a peak current of 10630 A. The triplet quadrupoles are powered by two nested power converters: one 8 kA power converter powering

all triplet quadrupole magnets in series and one 6 kA power converter supplying additional current only to the central two FNAL magnets. The Q1 quadrupole next to the IP features an additional 600 A trim power converter. The triplet quadrupoles are followed by the separation / recombination dipoles, D1 and D2, which guide the beams from the IP into two separated vacuum chambers. Q4, Q5, Q6, Q7, Q8, Q9 and Q10 are individually powered magnets. The aperture of Q4 is larger to provide sufficient aperture for the crossing-angle separation orbit. Two absorbers protect the cold magnets from particles leaving the IP. The TAS absorber protects the triplet quadrupole magnets and the TAN absorber, located in front of the D1 dipole magnet, protects the machine elements from neutral particles leaving the IP.

The matching section extends from Q4 to Q7 and the DS extends from Q8 to Q11. In addition to the DS, the first two trim quadrupoles of the first arc cell (QT12 and QT13) are also used for the matching procedure. All insertion and DS magnets are equipped with a beam screen [30]. The magnets left and right from the IP up to Q7 inclusive are placed symmetrically with respect to the IP. The positions of Q8, Q9 and Q10 left and right from the IP differ by approximately 0.5 m with respect to the IP due to the limited space in the DS.

3.2.5 IR2

The optics solutions in IR2 must obey a wide range of boundary conditions. A detailed description of these constraints can be found in reference [31].

The straight section at IR2 houses the injection elements for Ring-1 as well as the ion beam experiment ALICE. During injection the optics must obey the special constraints imposed by the beam injection for Ring-1 and the geometrical acceptance in the interaction region (IR) must be large enough to accommodate both beams in the common part of the ring with a beam separation of at least 10 σ.

IR layout

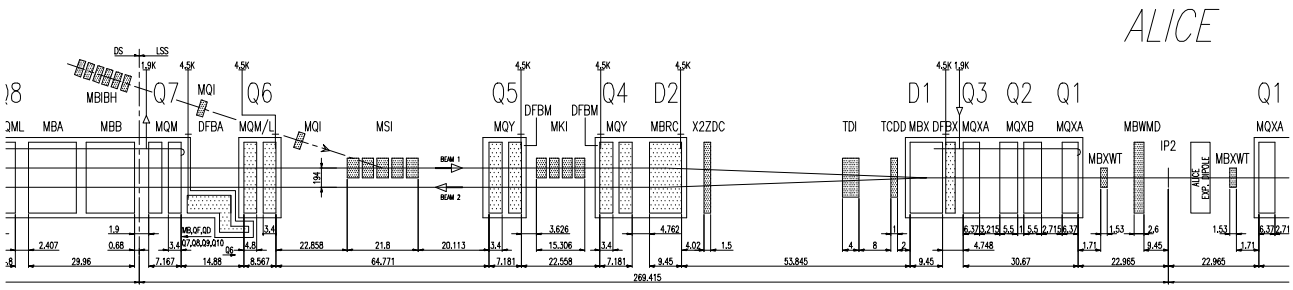

Figure 3.8: The left side of the matching section in IR2.

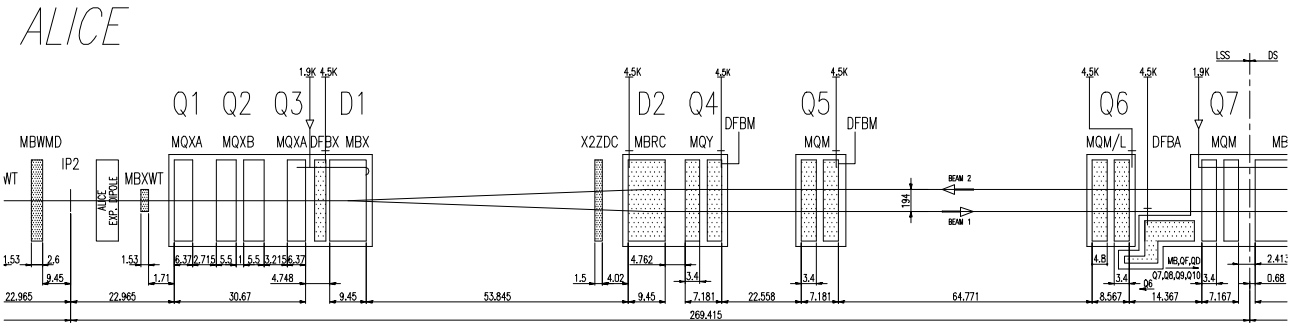

Figure 3.9: The right side of the matching section in IR2.

The triplet quadrupoles are powered in series and are followed by the separation / recombination dipoles D1 and D2, which guide the beams from the IP into two separated vacuum chambers. Q4, Q5, Q6, Q7, Q8, Q9 and Q10 are individually powered magnets. The aperture of Q4 is increased to provide sufficient aperture for the

crossing-angle separation orbit. The aperture of Q5 left of the IP is increased to provide sufficient aperture for the injected beam. The injection septum MSI is located between Q6 and Q5 on the left-side of the IP and kicks the injected beam in the horizontal plane towards the closed orbit of the circulating beam (positive deflection angle). The injection kicker MKI is located between Q5 and Q4 on the left-hand side of the IP and kicks the injected beam in the vertical plane towards the closed orbit of the circulating beam (negative deflection angle). In order to protect the cold elements in case of an injection failure a large absorber (TDI) is placed 15 m upstream from the D1 separation/recombination dipole left from the IP. The TDI absorber is complemented by an additional shielding element 3 m upstream of the D1 magnet and two additional collimators installed next to the Q6 quadrupole magnet. In order to obtain an optimum protection level in case of injection errors the vertical phase advance between MKI and TDI must be 90° and the vertical phase advance between the TDI and the two auxiliary collimators must be an integer multiple of $180^\circ \pm 20^\circ$.

The matching section extends from Q4 to Q7 and the DS extends from Q8 to Q11. In addition to the DS, the first two trim quadrupoles of the first arc cell (QT12 and QT13) are also used for the matching procedure. All magnets of the DS are equipped with a beam screen. The magnets left and right from the IP up to Q7 inclusive are placed symmetrically with respect to the IP. The positions of Q8, Q9 and Q10 left and right from the IP differ by approximately 0.5 m with respect to the IP due to the limited space in the DS.

Apart from the DS the insertions comprise the following sections, given in order from the interaction point:

- A 31 m long superconducting low-β triplet assembly operated at 1.9 K and providing a nominal gradient of 215 T/m.
- A pair of 9.45 m long superconducting separation / recombination dipole magnets separated by approximately 66 m.
- Four matching quadrupole magnets. The first two quadrupole magnets following the separation dipole magnets, Q4 and Q5, are wide aperture magnets operating at 4.5 K and yielding a nominal gradient of 160 T/m. The remaining two quadrupole magnets are normal aperture quadrupole magnets operating at 1.9 K with a nominal gradient of 200 T/m.

Figs 3.8 and 3.9 show the schematic layout of IR2 and Tab 3.3 summarizes its main hardware parameters.

Table 3.3: *Magnet parameters in IR2.*

	LSS								Optical DS					
	low-β triplet			MS					DS				arc-cell	
Magnet	Q1	Q2	Q3	Q4	Q5L	Q5R	Q6	Q7	Q8	Q9	Q10	QT11	QT12	QT13
#	1	2	1	2					1	2	1		1	
Type: MQ-	XL	X	XL	Y	Y	M	M		ML	M C	ML	TL	T	
L [m]	6.3	5.5	6.3	3.4					4.8	3.4 2.4	4.8	1.15	0.32	
T [K]	1.9			4.5			1.9		1.9				1.9	
B [T/m]	215 → 220			160			200		200			110	110	
r [mm]	22.2 17.3	28.95 24.05		27.2 22.3	27.2 22.3	20.6 15.75		22.2 17.3	22.2 17.3				22.2 17.3	

Hardware constraints

1. At the IP, the two rings of the LHC share the same vacuum chamber and the same low-beta triplet quadrupoles and the optics solutions for Ring 1 and Ring 2 must have the same triplet gradients.
2. The gradients must not exceed the maximum operating value (quench limit): 200 T/m for the insertion region quadrupoles at 1.9 K, 160 T/m for Q4 and Q5 which are operated at 4.5 K and 120 T/m for the trim

quadrupoles of the DS and 220 T/m for the triplet magnets without collisions (no heating from collision products) and 200 T/m with collisions at IP2.

3. The minimum gradient of the insertion quadrupoles which are powered by unipolar power converters must be larger than $3\ \%$ of the nominal gradient at injection energy.

4. The overall beam size must be small enough to fit into the tight aperture of the LHC. The aperture of the magnets is limited by the beam screen, and the aperture in the low-beta quadrupoles is further reduced by the vertical crossing-angle separation orbit. All magnets of the insertion are equipped with a race-track shaped beam screen, which is tilted by 90° wherever the required vertical aperture exceeds the required horizontal aperture. The aperture at the end of the MKI, the Q4 magnet and the D2 dipole magnet left from the IP, must be large enough to accommodate not only the circulating beam but also the mis-kicked injected and mis-kicked circulating beam.

3.2.6 IR3 and IR7

The insertion IR3 houses the momentum cleaning systems of both beams, while IR7 houses the betatron cleaning systems of both beams. Particles with a large momentum offset are scattered by the primary jaw of IR3. Particles with a large H, V or combined H-V betatron amplitudes are scattered by the primary collimator jaws in IR7. In both cases the scattered particles are absorbed by secondary collimators. The insertion layout and optics has been revised at the end of 2003 in order to reduce the impedance in the insertions and to make room for additional hybrid collimator jaws for the phase II of the LHC collimations system (see Chap. 18 for more details). The new layout drawings were not available at the time of writing. The layout given here therefore still corresponds to the old V6.4 lattice. However, all optics and aperture plots given in Chap. 4.2.4 and 4.2.7 correspond to the new optics that is based on the new layout and which will be part of the LHC V6.5 lattice.

IR7 layout

The dispersion suppressor extends from Q8 to Q11. In addition to the DS, the first two trim quadrupoles of the first arc cell (QT12 and QT13) are also used for the matching procedure. All cryo-magnets are equipped with a beam screen. In IR3 and IR7, the underground galleries are not wide enough to house many high current power supplies. Therefore, contrary to the layout of the other IR's, the DS quadrupoles (Q7,Q8,Q9 and Q10) are made of a MQ+MQTL assembly (MQ + 2 MQTL at Q9) where the MQ's magnets are powered in series with the main arc quadrupoles. To avoid producing two kinds of MQ+MQTL assemblies, the dispersion suppressors left and right from the IP are not mirror symmetric with respect to each other. Instead, the DS quadrupole assemblies have the same orientation in the dispersion suppressors left and right from the IP and the MQ positions differ by approximately 0.5 m with respect to the IP in the two DS.

The layout of the Long Straight Section between Q7L and Q7R is mirror symmetric with respect to the IP. The right side of IR7 is shown in Fig. 3.10. This allows the symmetrical installation for the collimators of the two beams and minimizes the space conflicts in the insertion. Starting from Q7 left, the quadrupole Q6 (made of 6 superconducting MQTL modules) is followed by a dog-leg structure made of two sets of MBW warm single bore wide aperture dipole magnets (2 warm modules each). The dogleg dipole magnets are labeled D3 and D4 in the LHC sequence with D3 being the dipole closer to the IP. The Primary Collimators are located between the D4 and D3 magnets, allowing neutral particles produced in the jaws to point out of the beam line, and most charged particles to be swept away. The inter-beam distance between the dogleg assemblies left and right from the IP is 224 mm, i.e. 30 mm larger than in the arc. This increased beam separation allows a substantially higher gradient in the Q4 and Q5 quadrupoles which are made out of 6 warm MQW modules. The space between Q5 left and right from the IP is used to house the secondary collimators at adequate phase advances with respect to the primary collimators.

The Q4 and Q5 quadrupoles left and right from the IP are powered in series. The warm dual-bore MQW quadrupole cannot be powered with different currents for each magnet aperture because the field quality is degraded to an unacceptable level even for a small imbalance in the field of the two apertures. The current

must be equal or of opposite value in the bores to provide a good field quality. In order to obtain the required flexibility for the optics, two different kinds of powering schemes are used for the Q4 and Q5 quadrupole units. The magnets are identical, but in the MQWA type magnet the field is identical in both apertures, $k_{\mathrm{Beam1}} = -k_{\mathrm{Beam2}}$ while in the MQWB type magnet, the field is opposite for both apertures, $k_{\mathrm{Beam1}} = k_{\mathrm{Beam2}}$ [32]. Each Q4 and Q5 assembly is made of 5 MQWA and 1 MQWB module. The nominal gradient of the MQWB unit is limited to 29.6 T/m while it can reach 35 T/m in the MQWA unit. This powering scheme breaks the exact antisymmetry by 29% providing enough flexibility to satisfy all the optics constraints. Again, Q5AL+Q5AR and Q5BL+Q5BR respectively are powered in series. As a by-product, this freedom in the straight section allows the trim strength needed in the DS to be limited so that regular MQTL's can be used. Fig. 3.10 shows the OLD V6.4 schematic layout of the right-hand side of IR7. A detailed description of the layout of the collimators can be found in Chap. 18 (this volume).

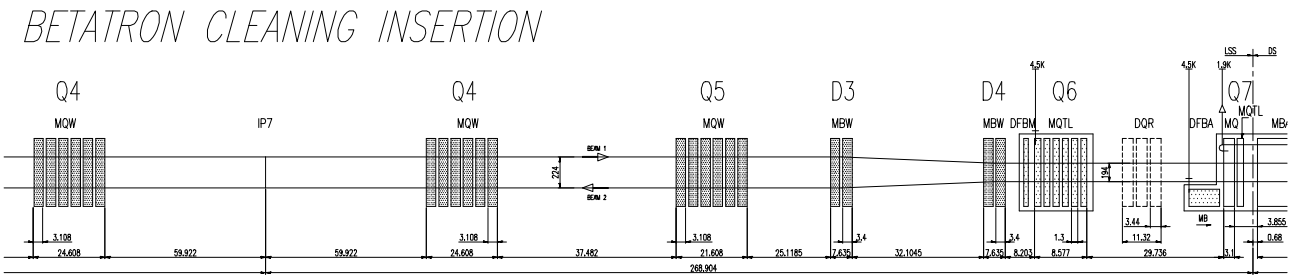

Figure 3.10: The right-hand side of the matching section in IR7.

IR3 layout

In IR3, the most difficult constraint was to generate a large dispersion function in the straight section. Since the layout of the DS cannot be changed in IR3 this constraint means that the natural dispersion suppression generated in the DS is over compensated. To this end Q6 and Q5 were moved towards each other by a substantial amount, thus shrinking the space granted to the dog-leg structure D4-D3. It was therefore necessary to add a third MBW element to D3 and D4 in IR3. Apart from this IR3 and IR7 are identical. Fig. 3.11 shows the OLD schematic layout of the right-hand side of IR3.

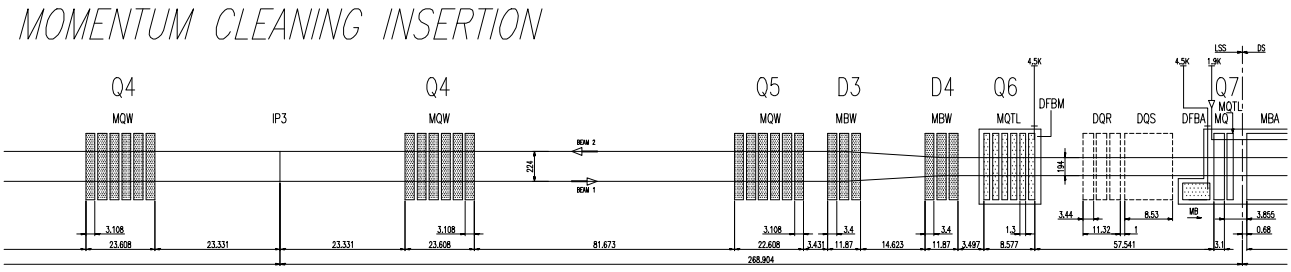

Figure 3.11: The right side of the matching section in IR3.

Hardware constraints

1. The MQWA may have gradients up to 35 T/m.
2. The MQWB may have gradients up to 29.6 T/m..
3. The maximum gradients must not exceed 120 T/m for the trim quadrupoles of the DS.
4. The overall beam size must be small enough to fit into the tight aperture of the LHC. The aperture of all cryo-magnets is limited by a beam screen, see Chap. 4.3. In the warm quadrupole the vacuum chamber

is elliptical with half main axis inner dimensions 25.5×14.5 mm. The shape of the vacuum chamber inside the MBW dipoles is not yet fixed. The present inner size has a race-track shape of half-dimensions 31.5×23 mm. This limits the maximum of the beta-functions to 400 m.

3.2.7 IR4

IR4 houses the RF and feed-back systems as well as some of the LHC beam instrumentation. In the first design described in the yellow book (the 1995 Conceptual Design)[14] the RF system was installed between Q5 and Q6 to leave room for an experiment. A detailed description of this insertion can be found in [33].

From 2001, the option of installing an experiment in IR4 has been dropped, allowing a simplification of the IR layout with respect to the previous version (e.g. to LHC V6.3). The RF is now installed in the ALEPH cavern, which provides a large space for the power supplies and klystrons. Because of the installation of both RF systems in this cavern, a large space is necessary between the quadrupole units surrounding the RF system. This makes the IR4 insertion look similar to the IR6 insertion. Furthermore, the two independent RF systems for Beam 1 and Beam 2 require a larger than nominal beam separation in the long straight section of IR4. The increased beam separation is provided by two pairs of dipole magnets. These dogleg dipole magnets are labeled D3 and D4 in the LHC sequence with D3 being the dipole magnets closer to the IP. The inter-beam distance between the dogleg magnets is 420 mm, i.e. 226 mm larger than in the arcs. In contrast to IR3 and IR7 the dogleg magnets in IR4 are superconducting magnets.

There are six superconducting quadrupole magnets in the straight section : Q5 Q6 Q7 on the left- and Q5 Q6 Q7 on the right-hand side of the IP. The outer dogleg dipoles, D4, sit next to the Q5 quadrupole magnets on each side of the IP. The RF cavities sit between the inner dogleg dipoles, D3. The layout of the DS, between Q7 and Q11, is identical to that in IR1 and IR5.

Fig. 3.12 shows the schematic layout of the right-hand side of IR4.

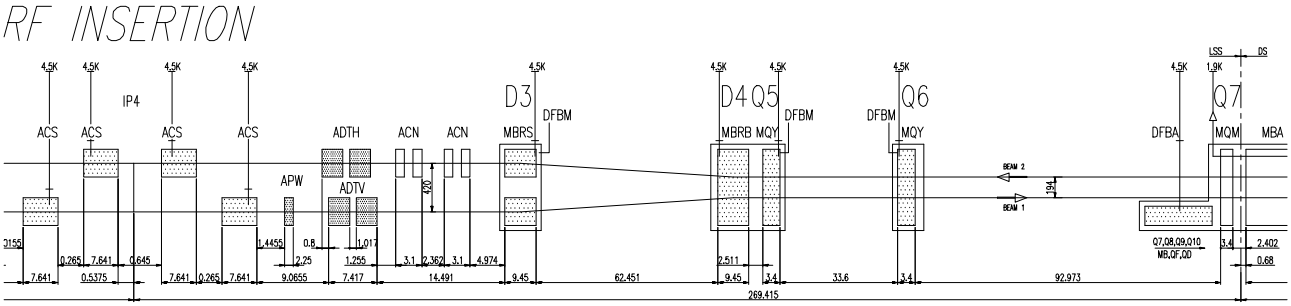

Figure 3.12: The right-hand side of the matching section in IR4.

3.2.8 IR6

IR6 houses the beam abort systems for Beam 1 and Beam 2. The beam extraction from the LHC is done by kicking the circulating beam horizontally into an iron septum magnet which deflects the beam in the vertical direction away from the machine components to absorbers in a separate tunnel. Each ring has its own system and both are installed in IR6.

In order to minimize the length of the kicker and the septum, large drift spaces have to be provided. Matching both β-functions between the ends of the left and right DS requires only four quadrupoles. Such a scheme was used in the first design [34] which was proposed a long time ago. Later on quadrupoles were added to achieve a phase advance equal to that of the other insertions, this was LHC Version 1 [35]. Eventually the design of the components of the beam dump system was based on similar optics labeled V4 [14].

For the nominal version 6 optics, there are four quadrupoles independently powered in the straight section of the insertion. This independent powering is possible as the gradients in the two apertures of the quadrupoles can have different values, i.e. they are no longer constrained to be exactly opposite, which was the case for LHC version 4. Fig. 3.13 shows the schematic layout of the right-hand side of IR6.

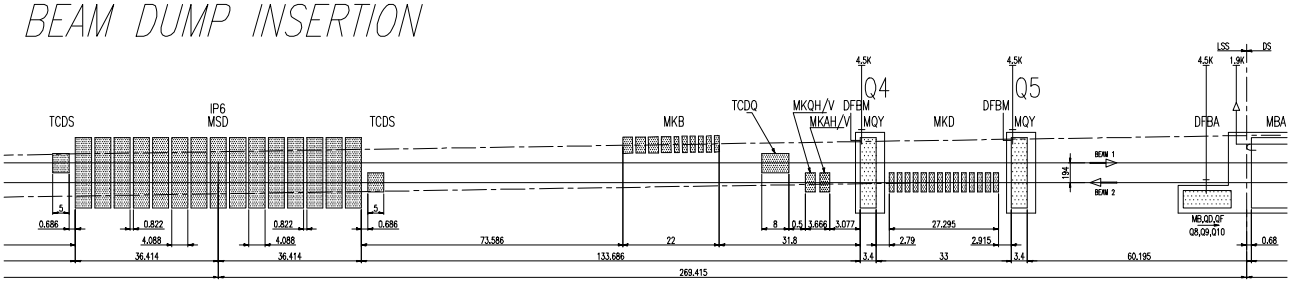

Figure 3.13: The right-hand side of the matching section in IR6.

In each of the dispersion suppressors up to six quadrupoles can be used for matching. The total of sixteen quadrupoles is more than necessary to match both β-functions, the dispersion (both at the crossing point and in the arc) and adjust the phases. Although this number of parameters seems considerable, their variation is strongly limited by the aperture constraints which set limits on the β-functions and the dispersion inside the insertion. Special detection devices protect the extraction septum and the LHC machine against losses during the extraction process. The TCDS absorber is located in front of the extraction septum and the TCDQ in front of the Q4 quadrupole magnet downstream of the septum magnet.

3.2.9 IR8

General description

IR8 houses the LHCb experiment and the injection elements for Beam 2. The small β-function values at the IP are generated with the help of a triplet quadrupole assembly [19]. A detailed description of the matching constraints for IR8 can be found in [36]. The free space around the IPs is ± 23 m and the Q1 magnet now stands in the tunnel instead of being supported by a cantilever inside the experimental cavern. At the IP, the two rings share the same vacuum chamber, the same low-beta triplet magnets and the D1 separation dipole magnet. The remaining matching section (MS) and the DS consist of double-bore magnets with separate beam pipes for each ring.

IR layout

Apart from the DS the insertions contain the following sections, given in order from the interaction point:

- Three warm dipole magnets compensate the deflection generated by the LHCb spectrometer magnet.
- A 31 m long superconducting low-β triplet assembly operated at 1.9 K and providing a nominal gradient of 205 T/m.
- A pair of separation/recombination dipole magnets separated by approximately 54 m. The D1 dipole located next to the triplet magnets is a 9.45 m long single-bore superconducting magnet. The following D2 dipole is a 9.45 m long, double bore, superconducting dipole magnet. Both magnets are operated at 4.5 K. The bore separation in the D2 magnet is 188 mm and is thus slightly smaller than the arc bore separation.
- Four matching quadrupole magnets. The first quadrupole following the separation dipole magnets, Q4, is a wide aperture magnet operating at 4.5 K and yielding a nominal gradient of 160 T/m. The remaining three matching section quadrupole magnets are normal aperture quadrupole magnets operating at 1.9 K with a nominal gradient of 200 T/m.
- The injection elements for Beam 2 on the right hand side of IP8. The 21.8 m long injection septum consists of 5 modules and is located between the Q6 and Q5 quadrupole magnets on the right-hand side of the IP. The 15 m long injection kicker consists of 4 modules and is located between the Q5 and Q4 quadrupole

magnets on the right-hand side of the IP. In order to protect the cold elements in case of injection failure a large absorber (TDI) is placed 15 m in front of the D1 separation/recombination dipole magnet right from the IP. The TDI is complemented by an additional shielding element between the TDI and D1 magnet (placed 3 m in front of D1) (TCDD) and by two additional collimators placed on the transition of the matching section left from the IP to the next DS section.

In order to provide sufficient space for the spectrometer magnet of the LHCb experiment IP8, is shifted by 15 half RF wavelengths (3.5 times the nominal bunch spacing $\rightarrow\approx 11.25$ m) towards IR7. This shift of the IP has to be recuperated before the beam returns to the dispersion suppressor sections and implies a non-symmetric magnet layout in the matching section.

Fig. 3.14 and 3.15 show the schematic layout of IR8 and Tab 3.4 summarizes the main hardware parameters.

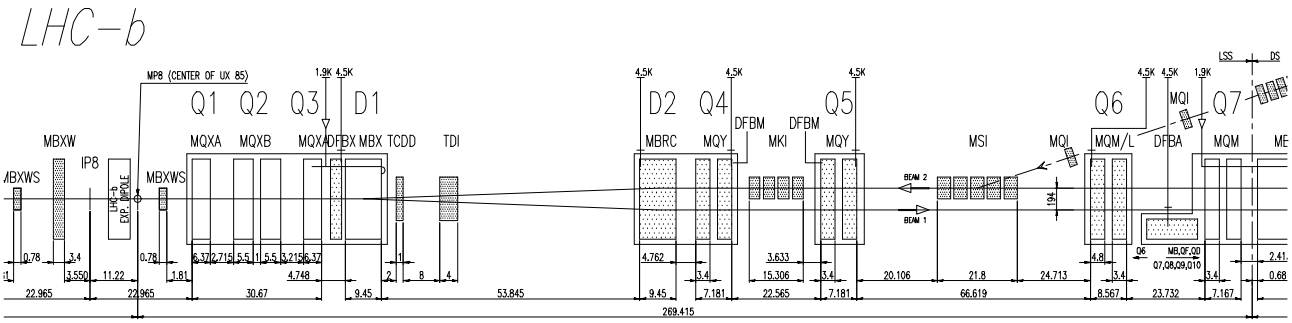

Figure 3.14: Schematic layout of the right side of IR8

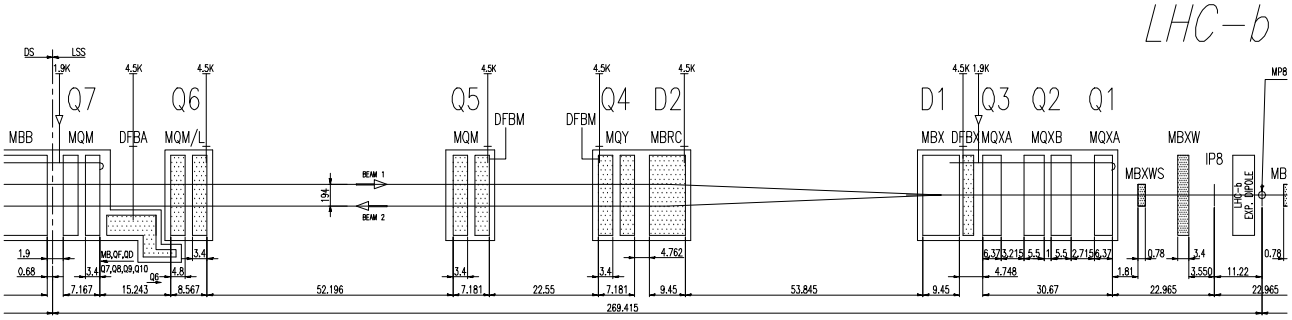

Figure 3.15: Schematic layout of the left side of IR8

Table 3.4: *Quadrupole magnet parameters in IR8.*

	LSS								Optical DS					
	low-β triplet			MS					DS				arc-cell	
Magnet	Q1	Q2	Q3	Q4	Q5R	Q5L	Q6	Q7	Q8	Q9	Q10	QT11	QT12	QT13
#	1	2	1	2					1	2	1		1	
Type: MQ-	XL	X	XL	Y	Y	M	M		ML	M C	ML	TL	T	
L [m]	6.3	5.5	6.3	3.4					4.8	3.4 2.4	4.8	1.15	0.32	
T [K]	1.9			4.5			1.9		1.9				1.9	
B [T/m]	$215 \rightarrow 220$			160			200		200			110	110	
r [mm]	22.2 17.3	28.95 24.05		27.2 22.3	27.2 22.3	20.6 15.75		22.2 17.3	22.2 17.3				22.2 17.3	

The triplet assembly features two different quadrupole designs: the two outer quadrupole magnets are made by KEK and require a peak current of 6450 A for reaching the nominal gradient of 205 T/m and the inner quadrupole block consists of two quadrupole magnets made by FNAL and requires a peak current of 10630 A. The triplet quadrupoles are powered by two nested power converters. One 8 kA power converter powering all triplet quadrupole magnets in series and one 6 kA power converter supplying additional current only to the central two FNAL magnets. [4] The triplet quadrupoles are followed by the separation/recombination dipoles, D1 and D2, which guide the beams from the IP into two separated vacuum chambers. Q4, Q5, Q6, Q7, Q8, Q9 and Q10 are individually powered magnets. The apertures of Q4 and Q5 are increased to provide sufficient aperture for injected beam and the crossing-angle separation orbit.

The matching section extends from Q4 to Q7 and the DS extends Q8 to Q11. In addition to the DS, the first two trim quadrupoles of the first arc cell (QT12 and QT13) are also used for the matching procedure. All insertion and DS magnets are equipped with a beam screen [30]. The positions of Q8, Q9 and Q10 left and right from the IP differ by approximately 0.5 m with respect to the IP due to the limited space in the DS.

REFERENCES

[1] LEP Design Report; CERN-LEP/84-01; June 1984 and CERN-AC/96-01 (LEP2); June 1996

[2] ATLAS Technical Proposal; CERN / LHCC / 94-43; LHCC / P2; December 1994

[3] CMS Technical proposal; CERN-LHCC-94-38; LHCC-P-1; December 1994

[4] LHCB Technical Proposal; CERN/LHCC 98-4; February 1998

[5] Total Cross Section, Elastic Scattering and Diffractive Dissociation at the LHC, CERN / LHC 99-7, March 1999

[6] ALICE Technical Prposal; CERN/LHCC 95-71; December 1995

[7] H. Grote and W. Herr, Nominal and Ultimate Luminosity Performance of the LHC, LHC Project Note 275, January 2002

[8] Design Study of the Large Hadron Collider, CERN/91-03, 1991

[9] LHC Luminosity and Energy Upgrade: A Feasibility Study; LHC Project Report 626, December 2002

[10] O. Gröbner, 'Overview of the LHC Vacuum System', VACUUM **60**, pg. 25-34, 2001

[11] O. Brüning in the Chamonix 2000 proceedings

[12] A. Faus-Golfe, LHC Project Note 9, 1995

[13] O. Brüning in the Chamonix 2001 proceedings

[14] The LHC study group, The LARGE HADRON COLLIDER Conceptual design. CERN/AC/95-05(LHC), 20 October 1995.

[15] J.P. Koutchouk, Presentation to the 4. LHC Machine Advisory Committee 24/06/97

[16] A.Faus-Golfe, H. Grote, J-P Koutchouk, T. Risselada, A. Verdier, S. Weisz, 'A more robust and flexible lattice for LHC', LHC Project Report 107, 1997, and in the proceedings of PAC97, Vancouver, Canada

[17] Oliver Brüning, Presentation at the 10. LHC Machine Advisory Committee, http://slap.web.cern.ch/slap/MAC.pdf

[18] J.P. Koutchouk, W. Scandale and A. Verdier, Optimization of the LHC Lattice and Chromaticity. Proc. of the IEEE Part. Acc. Conf. Washington DC, March 1987.

[19] E. Keil, CERN 77-13, 1977 or R. Brinkmann, Insertions, CAS proceedings, pg. 45-61, CERN 87-10, Aarhus, Denmark, July 1987

[20] A. Faus-Golfe, J-P Koutchouk, A Verdier and S. Weisz, Modular Optics Design of the LHC Experimental Insertions, LHC Project Report 14, 1996 and in the proceedings of the EPAC96, Barcelona, Spain

[21] J.P. Koutchouk, Presentation to the 6. LHC Machine Advisory Committee 2/11/1998.

[22] A. Verdier, Revision of the Closed Orbit Corrector System of the LHC, CERN-LHC-Project-Report-397, Geneva, CERN (August 1, 2000).

[4] The Q1 quadrupole next to the IP features an additional 600 A trim power converter.

[23] S. Fartoukh, Second order chromaticity correction of LHC V6.0 at collision, LHC-Project-Report-308, Geneva, CERN (October, 1999).

[24] F. Schmidt, “Strength Requirements for the Arc Sextupoles of LHC Version 4.1”, LHC Project Note 38

[25] S. Fartoukh, Chromatic coupling induced by skew sextupolar field errors in the LHC main dipoles and its correction, LHC-Project-Report-278, Geneva, CERN (March 1999).

[26] A. Verdier, Operational Q-shifts and $b2$ compensation in LHC, CERN-LHC-Project-Note-26, Geneva, CERN (January 8, 1996).

[27] O. Brüning, Linear coupling compensation for the LHC Version 6.1, EPAC 2000 Proc., 26-30 June 2000, Vienna and LHC-Project-Report-399, Geneva, CERN (August, 2000).

[28] J. Gareyte, J.P. Koutchouk, F. Ruggiero, Landau Damping, Dynamic Aperture and Octupoles in LHC, LHC-Project-Report-91 (revised), Geneva, CERN (April, 1997).

[29] O. Brüning, Optics Solutions in IR1 and IR5 for Ring-1 and Ring-2 of the LHC Version 6.0; 5LHC Project Note 187, April 1999

[30] 33. LCC meeting held on 20.11.2002: http://lhcp.web.cern.ch/lhcp/LCC/LCC_2002-18.htm

[31] O. Brüning, Optics Solutions in IR2 for Ring-1 and Ring-2 of the LHC Version 6.0; LHC Project Note 188, April 1999

[32] D.I. Kaltchev et al., M.K. Craddock, J.B. Jeanneret and A. Verdier, LHC Project Report 305 and PAC1999,1999.

[33] A. Verdier, A tunable insertion for point 4 in LHC. LHC Project Note 93 (June 1997).

[34] The large hadron collider in the LEP tunnel. Edited by G. Brianti and K. Hűbner. CERN 87-05 (27 May 1987).

[35] Design study of the Large Hadron Collider, The LHC study group, CERN 91-03.

[36] O. Brüning, Optics Solutions in IR8 for Ring-1 and Ring-2 of the LHC Version 6.0; LHC Project Note 193, June 1998